Modified force method for the nonlinear analysis of FRP reinforced concrete beams

Massimiliano Bocciarelli *, Marco Andrea Pisani

Department of Architecture, Built Environment and Construction Engineering, Politecnico di Milano, piazza Leonardo da Vinci 32, 20133, Italy

Available online 6 June 2015

1. Introduction

Advanced fiber reinforced composite materials have been used for many years in civil engineering for structural retrofitting of both reinforced concrete and steel elements, in view of their particularly useful properties: corrosion resistance, high strength, low dead weight and hence ease-to-use which avoids the cumbersome work associated with traditional retrofitting techniques, see [1–4].

Composite materials may be used for different purposes: flexural strengthening of both reinforced concrete (RC) and steel beams, as in [5–7]; shear strengthening of RC elements, see [8–10]; prevent local buckling of steel beams web, see [11]; strengthening of tensile steel elements under fatigue and static loading, as in [12–15] and confinement of RC columns, see [16,17].

When dealing with this type of strengthening, one of the main issues, which may prevent to achieve the full load bearing capacity of the retrofitted element, is the debonding of the CFRP lamina from the substrate. In addition, even before failure, significant slip occurs at the interface, (see, e.g. [18–21]), which affects the service behavior of the retrofitted elements and prevents from analyzing them according to the usual hypothesis of conservation of plane section, unless simplified and safe assumptions are formulated, as in [22,23].

Different numerical studies, that take into account the partial interaction between CFRP reinforcement and substrate, based on 1D (see for instance [24]), 2D (see [25,26]) and 3D (see [27–29]) finite element formulations exist in literature. Partial interaction modeling is also considered in composite beams to take into account separately the behavior of both concrete slab and steel beam, see for instance [30,31]. All the approaches, proposed to model externally reinforced beams, predict fairly well the behavior under service loads, but most of them fail in the prediction of the ultimate load or highlight the impossibility in following the debonding phenomena occurring at the interface up to the complete detachment of the reinforcement lamina.

This paper presents a novel numerical approach, based on the force method, in which the response of an externally reinforced beam is derived by enforcing compatibility along the interface between concrete and CFRP lamina. However, in view of the softening nature of the cohesive law governing the response of the interface, the usual approach to the force method was modified and the problem was formulated assuming as primary unknowns the interface slips, instead of the interface shear stresses. It is demonstrated that this approach is stable enough to follow, unless snap-back occurs, the complete equilibrium path from the

* Corresponding author. Tel.: +39 0223994320; fax: +39 0223994369.
E-mail address: massimiliano.bocciarelli@polimi.it (M. Bocciarelli).

response of the strengthened beam to that of the original one after the debonding of the external reinforcement and the consequent and sudden load drop.

The problem formulation brings to a set of nonlinear equations, which are solved within a classical Newton–Raphson scheme, whose corresponding consistent tangent operator is derived.

The paper is organized as follows: Section 2 describes the numerical method proposed to compute the response of an externally reinforced beam. Then results of the modeling of benchmarking experimental tests taken from literature are derived in Section 3 in order to validate the proposed numerical approach. Section 4 presents some parametric analyses aimed at showing the effect of the main design parameters on the overall behavior of a RC beam retrofitted by a CFRP lamina. Finally, conclusion, highlighting potentialities and limitation of the proposed method, are drawn in Section 5.

2. Numerical method

The numerical method, proposed to model an externally reinforced concrete beam, see Fig. 1, is based on the following assumptions:

- beam sections possess an axis of symmetry perpendicular to moment axis and remain plane during deformation;
- perfect bond is assumed between concrete and steel rebars;
- slips occurring at the interface between the concrete substrate and the external reinforcement are governed by a cohesive law with softening behavior;
- concrete, steel rebars and external reinforcement behave as nonlinear materials;
- bending stiffness of external reinforcement is negligible.

2.1. Constitutive equations

A brittle nonlinear elastic constitutive behavior is assumed for the external reinforcement (usually a Carbon Fibre Reinforced Polymer, or a Glass Fibre Reinforced Polymer), see Fig. 2:

$$\sigma_r = \begin{cases} H(\varepsilon_r)\cdot E_r\varepsilon_r & \text{if } \varepsilon_r \leqslant \varepsilon_{ru} \\ 0 & \text{if } \varepsilon_r > \varepsilon_{ru} \end{cases} \tag{1}$$

where: σ_r and ε_r are the axial stress and strain, respectively, E_r is the corresponding Young modulus, ε_{ru} is the ultimate strain and $H(\varepsilon_r)$ is the Heaviside step function.

Reference is made to reinforced concrete beams to formulate the proposed approach. For concrete in compression the classical parabola-rectangle stress–strain relationship, see [32], is considered, while the behavior of concrete under tensile stress is assumed to be linear elastic up to the tensile strength f_{ct} and then it drops to zero, see Eq. (2) and Fig. 3:

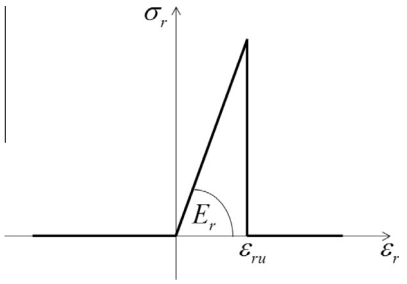

Fig. 2. Stress–strain relationship assumed for FRP.

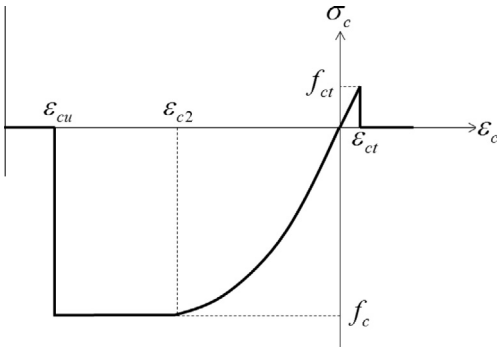

Fig. 3. Stress–strain relationship assumed for concrete.

$$\sigma_c = \begin{cases} 0 & \text{if } \varepsilon_c > \varepsilon_{ct} \\ E_c\varepsilon_c & \text{if } 0 \leqslant \varepsilon_c \leqslant \varepsilon_{ct} \\ \dfrac{\varepsilon_c}{\varepsilon_{c2}}\left(2+\dfrac{\varepsilon_c}{\varepsilon_{c2}}\right)f_c & \text{if } -\varepsilon_{c2} \leqslant \varepsilon_c < 0 \\ -f_c & \text{if } -\varepsilon_{cu} \leqslant \varepsilon_c < -\varepsilon_{c2} \\ 0 & \text{if } \varepsilon_c < -\varepsilon_{cu} \end{cases} \tag{2}$$

where: $\varepsilon_{c2} = 0.002$ is the strain at the end of the parabola, ε_{cu} is the ultimate compressive strain and $\varepsilon_{ct} = f_{ct}/E_c$ represents the tensile mechanical strain at the peak stress f_{ct}.

For internal steel reinforcement a classical elasto-plastic constitutive law is adopted with isotropic linear hardening, that is:

$$\sigma_s = \begin{cases} E_s\varepsilon_s & \text{if } |\varepsilon_s| \leqslant f_{sy}/E_s \\ \left[f_{sy} + H_s\left(|\varepsilon_s| - f_{sy}/E_s\right)\right]\cdot\dfrac{\varepsilon_s}{|\varepsilon_s|} & \text{if } f_{sy}/E_s \leqslant |\varepsilon_s| \leqslant \varepsilon_{su} \\ 0 & \text{if } |\varepsilon_s| > \varepsilon_{su} \end{cases} \tag{3}$$

where: σ_s and ε_s are the steel axial stress and strain, respectively, f_{sy} the yield stress and E_s, H_s the steel Young modulus and the linear hardening coefficient, respectively.

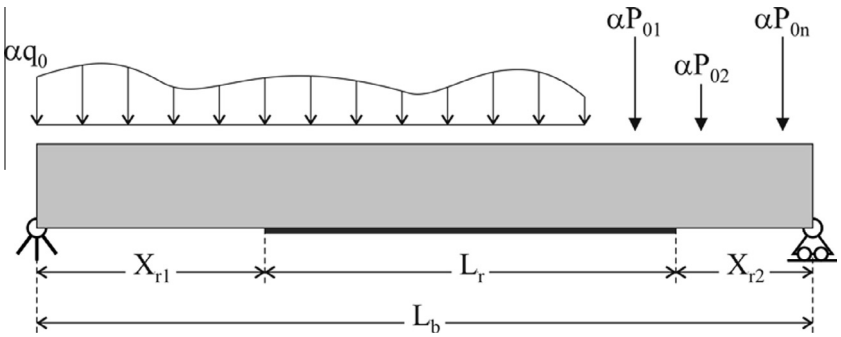

Fig. 1. Illustrative representation of a beam externally reinforced in bending with a CFRP lamina.

The cohesive law adopted to model the interface between the beam and the external reinforcement, i.e. the relationship between interface shear stress t and slip s, is the classical bilinear one, see [22] and Fig. 4, described in the following equation:

$$t = \begin{cases} K_f s & \text{if } 0 \leqslant s \leqslant s_e \\ t_f - \dfrac{s - s_e}{s_u - s_e} t_f & \text{if } s_e \leqslant s \leqslant s_u \\ 0 & \text{if } s > s_u \end{cases} \tag{4}$$

The above cohesive law depends on three parameters: the interface shear strength t_f, the elastic stiffness K_f and the fracture energy G_f (i.e. the area under the curve).

2.2. Reinforced concrete cross-section behavior

In the present Section, the procedure adopted to construct the three dimensional surfaces, relating both the curvature χ_b and axial deformation η_b (defined with respect to the center of gravity G of the geometric cross section, see Fig. 5) of the beam section to the bending moment M_b and axial force N_b, will be described.

According to the above hypotheses and to the assumptions in Fig. 5, the compatibility equation governing the response of the concrete beam section can be written as follows:

$$\varepsilon_c(y) = \eta_b - \chi_b \cdot y \tag{5}$$

Given an axial force N_b and a curvature χ_b, the horizontal equilibrium is imposed as:

$$N(\eta_b) = \int_{A_c} \sigma_c(\varepsilon_c(\eta_b))dA + \sum_k \sigma_{sk}(\varepsilon_{sk}(\eta_b)) \cdot A_{sk} = N_b \tag{6}$$

where A_{sk} is the area of the kth rebar and σ_{sk} the corresponding stress.

Integration over the cross section can be carried out either by performing an analytical integration (see [33,34]), or by adopting a numerical quadrature formula (namely Gauss' formula, see [35]). Nevertheless, because of the former assumption that the beam section possesses an axis of symmetry perpendicular to moment axis, a simple numerical quadrature formula based on the discretization of the cross section in horizontal strips (see for instance [36]) is adopted, that is:

$$N(\eta_b) = \sum_j \sigma_{cj}(\varepsilon_{cj}(\eta_b)) \cdot A_{cj} + \sum_k \sigma_{sk}(\varepsilon_{sk}(\eta_b)) \cdot A_{sk} = N_b \tag{7}$$

where: ε_{cj} is the strain computed by means of Eq. (5) in the center of gravity (placed at ordinate y_j) of each jth horizontal strip of area A_{cj} and σ_{cj} is the corresponding stress computed trough Eq. (2). In view of the assumed perfect bond between concrete and steel reinforcement, we get $\varepsilon_{sk}(\eta_b) = \varepsilon_c(\eta_b)|_{y=y_{sk}}$.

Eq. (6) is non-linear in the unknown η_b, but the choice of discretize it by means of Eq. (7) makes it easy to adopt an iterative formula based on the Newton–Raphson scheme:

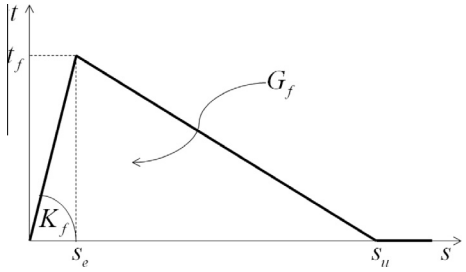

Fig. 4. Bilinear cohesive law adopted to model the interface behavior.

$$N|_{\eta_b^{i+1}} = N|_{\eta_b^i} + \left.\frac{dN}{d\eta_b}\right|_{\eta_b^i} \cdot (\eta_b^{i+1} - \eta_b^i) = N_b \rightarrow \eta_b^{i+1} = \eta_b^i - \frac{\left[N|_{\eta_b^i} - N_b\right]}{\left.\frac{dN}{d\eta_b}\right|_{\eta_b^i}} \tag{8}$$

where η_b^i and $N|_{\eta_b^i}$ are the trial and the corresponding axial stress resultant at the ith iteration, respectively; while in view of Eq. (7), the derivative reads:

$$\left.\frac{dN}{d\eta_b}\right|_{\eta_b^i} \overset{\frac{d\varepsilon_c}{d\eta_b} = \frac{d\varepsilon_s}{d\eta_b} = 1}{=} \sum_j \left.\frac{d\sigma_c}{d\varepsilon_c}\right|_{\varepsilon_{cj}^i} \cdot A_{cj} + \sum_k \left.\frac{d\sigma_s}{d\varepsilon_s}\right|_{\varepsilon_{sk}^i} \cdot A_{sk} \tag{9}$$

where $\left.\frac{d\sigma_c}{d\varepsilon_c}\right|_{\varepsilon_{cj}^i}$ and $\left.\frac{d\sigma_s}{d\varepsilon_s}\right|_{\varepsilon_{sk}^i}$ are the current tangent moduli of the concrete and steel constitutive laws, respectively.

Once that the value of η_b has been computed the strain distribution is known and through the constitutive equations (2) and (3) the moment M_b corresponding to the given axial force N_b and curvature χ_b can be derived as follows:

$$M_b = -\int_A \sigma_c(\varepsilon_c) y dA - \sum_k \sigma_{sk}(\varepsilon_{sk}) y_{sk} A_{sk} \tag{10}$$

that is

$$M_b = -\sum_j \sigma_c|_{\varepsilon_c = \eta_b - \chi_b \cdot y_{cj}} y_{cj} A_{cj} + \sum_k \sigma_s|_{\varepsilon_s = \eta_b - \chi_b \cdot y_{sk}} y_{sk} A_{sk} \tag{11}$$

Finally the position X of the neutral axis (with respect to the upper part of the section, see Fig. 5) can be computed as follows:

$$X = H - y_G - \frac{\eta_b}{\chi_b} \tag{12}$$

By repeating the above passages for all the combinations of given sets of axial forces and curvatures the sought surfaces can be built numerically.

Since these surfaces are derived in a discrete form; we describe now the method adopted to compute the values $\left(\chi_b, \frac{\partial \chi_b}{\partial N_b}, \frac{\partial \chi_b}{\partial M_b}\right)$ and $\left(\eta_b, \frac{\partial \eta_b}{\partial N_b}, \frac{\partial \eta_b}{\partial M_b}\right)$ for any value of (N_b, M_b), needed to achieve the structural response according to the formulation described in the next Section.

Within the above defined discretized surfaces we first find the triples (χ_{11}, N_1, M_1), (χ_{12}, N_1, M_2), (χ_{21}, N_2, M_1) and (χ_{22}, N_2, M_2) such that: $N_1 \leqslant N_b \leqslant N_2$ and $M_1 \leqslant M_b \leqslant M_2$, see Fig. 6. Then the following approximation is adopted:

$$\begin{cases} \chi_b \approx aN_b + bM_b + cN_bM_b + d \\ \dfrac{\partial \chi_b}{\partial N_b} \approx a + cM_b, \dfrac{\partial \chi_b}{\partial M_b} \approx b + cN_b \end{cases} \text{where:} \begin{bmatrix} N_1 & M_1 & N_1M_1 & 1 \\ N_2 & M_1 & N_2M_1 & 1 \\ N_2 & M_2 & N_2M_2 & 1 \\ N_1 & M_2 & N_1M_2 & 1 \end{bmatrix} \begin{bmatrix} a \\ b \\ c \\ d \end{bmatrix} = \begin{bmatrix} \chi_{11} \\ \chi_{21} \\ \chi_{22} \\ \chi_{12} \end{bmatrix} \tag{13}$$

The same method is applied to compute $\left(\eta_b, \frac{\partial \eta_b}{\partial N_b}, \frac{\partial \eta_b}{\partial M_b}\right)$.

2.3. Evaluation of the structural response

The beam is first discretized in M-1 segments. Each element, between two nodes, is then split in two parts: the reinforced concrete beam segment and the external reinforcement one, whose interaction depends on the interface shear stresses t (see Fig. 7).

The numerical method adopted aims at simulating the response of a CFRP reinforced beam in a loading test. Debonding of the external reinforcement from the substrate is usually very brittle and induces a sudden decrease of the stiffness and of the load-carrying capacity of the beam. In order to model this process

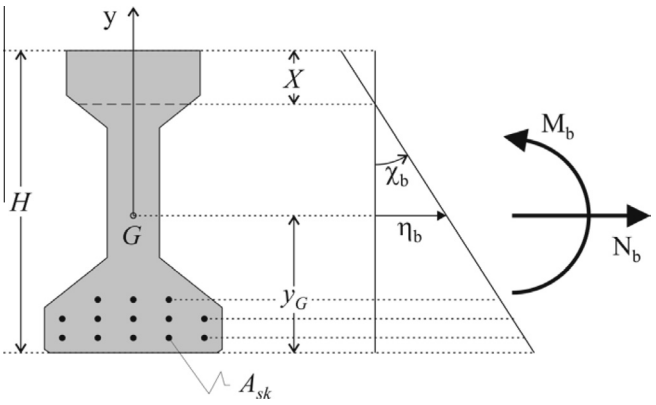

Fig. 5. Generic section of the reinforced beam having an axis of symmetry.

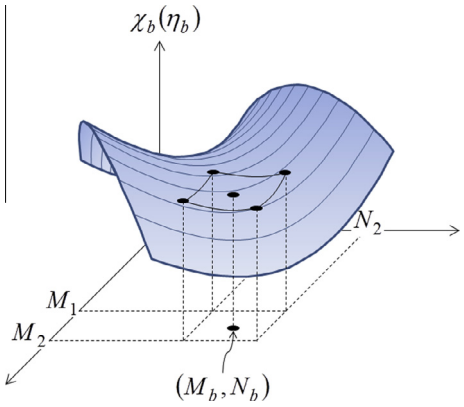

Fig. 6. Illustrative representation of the surfaces relating the curvature χ_b and the axial deformation η_b to the bending moment M_b and axial force N_b.

a displacement controlled numerical procedure is adopted. At each kth loading step an increasing value $\delta_{m,k}$ of the displacement at a certain section m of the beam is assigned (in the following defined as controlling point). All external loads (else than the self-weight) will then gradually increase, proportionally to a factor named α_k, up to the ultimate load and then will suddenly decrease when further increasing $\delta_{m,k}$. The load factor α_k needed to achieve the applied displacement $\delta_{m,k}$ is one of the unknowns.

The solution is searched also in terms of unknown interface slips $\mathbf{s}_k = [s_{1,k} \quad \dots \quad s_{N,k}]^T$ (N being the number of nodes used to discretize the interface, see Fig. 7). Once vector $\mathbf{s}_k$ is known, the corresponding interface shear stresses $\mathbf{t}_k = [t_{1,k} \quad \dots \quad t_{N,k}]^T$ can be derived through the adopted cohesive law, see Eq. (4). The vectors of bending moment $\mathbf{M}_{b,k} = [M_{b1,k} \quad \dots \quad M_{bM,k}]^T$ and axial force $\mathbf{N}_{b,k} = [N_{b1,k} \quad \dots \quad N_{bM,k}]^T$ in the beam, and axial force $\mathbf{N}_{r,k} = [N_{r1,k} \quad \dots \quad N_{rN,k}]^T$ in the external reinforcement, could then be derived by simple equilibrium equations in the generic section j as:

$$\begin{aligned} M_{bj,k} &= M_{bj,\alpha_k} - b(y_G + y_R)\left\langle \sum_{i=1}^{f(j)} t_{i,k}\Delta x_i \right\rangle \quad \forall j = 1 \dots M \\ N_{bj,k} &= N_{bj,\alpha_k} - b\left\langle \sum_{i=1}^{f(j)} t_{i,k}\Delta x_i \right\rangle \quad \forall j = 1 \dots M \\ N_{rj,k} &= b\left\langle \sum_{i=1}^{f(j)} t_{i,k}\Delta x_i \right\rangle \quad \forall j = 1 \dots N \end{aligned} \tag{14a, b, c}$$

where the term in brackets $\langle \cdots \rangle$ is equal to zero for those sections not externally reinforced, $f(j)$ is the upper limit of the summation, function of the section j where the internal forces are computed, b is the external reinforcement width, index α_k refers to the contribution of the external loads, and y_R is the distance between the center of gravity of the CFRP reinforcement and the bottom of the reinforced concrete cross section (see Fig. 7). As soon as the distribution of the internal forces is assessed it is possible to compute, through Eqs. (1) and (13), the characteristics of deformation of both concrete beam and external reinforcement sections:

$$\begin{aligned} \chi_{bj,k} &= \chi_b(M_{bj,k}, N_{bj,k}) \\ \eta_{bj,k} &= \eta_b(M_{bj,k}, N_{bj,k}) \\ \eta_{rj,k} &= \eta_r(N_{rj,k}) \end{aligned} \tag{15a, b, c}$$

and the corresponding vectors defined as follows: curvature $\boldsymbol{\chi}_{b,k} = [\chi_{b1,k} \quad \cdots \quad \chi_{bM,k}]^T$ and axial deformation $\boldsymbol{\eta}_{b,k} = [\eta_{b1,k} \quad \cdots \quad \eta_{bM,k}]^T$ in the concrete beam and axial deformation $\boldsymbol{\eta}_{r,k} = [\eta_{r1,k} \quad \cdots \quad \eta_{rN,k}]^T$ in the reinforcement.

By integration of the above beam and reinforcement deformations and by the use of the principle of virtual work, it is possible to compute: the vectors of concrete beam sections axial displacements $\mathbf{u}_{b,k} = [u_{b1,k} \quad \dots \quad u_{bM,k}]^T$ and rotations $\boldsymbol{\theta}_{b,k} = [\theta_{b1,k} \quad \dots \quad \theta_{bM,k}]^T$, the vector of the external reinforcement axial displacements $\mathbf{u}_{r,k} = [u_{r1,k} \quad \dots \quad u_{rN,k}]^T$ and the transversal displacement $v_{bm,k}$ at the controlling point, i.e. the section m where the displacement $\delta_{m,k}$ is imposed:

$$\begin{aligned} u_{bj,k} &= \sum_{i=1}^{j} \eta_{bi,k}\Delta x_i \\ \theta_{bj,k} &= \sum_{i=1}^{M} \hat{M}_i^1 \chi_{bi,k}\Delta x_i + \sum_{i=1}^{j} \chi_{bi,k}\Delta x_i \\ u_{rj,k} &= u_{r1,k} + \sum_{i=1}^{j} \eta_{ri,k}\Delta x_i \\ v_{bm,k} &= \sum_{i=1}^{M} \hat{M}_i^m \chi_{bi,k}\Delta x_i \end{aligned} \tag{16a, b, c, d}$$

where $\hat{\mathbf{M}}^1 = [\hat{M}_1^1 \quad \dots \quad \hat{M}_M^1]^T$ and $\hat{\mathbf{M}}^m = [\hat{M}_1^m \quad \dots \quad \hat{M}_M^m]^T$ are the bending moment distributions due to a unit couple applied at the left end section and to a unit force applied at the specific coordinate where the displacement $\delta_{m,k}$ is imposed, respectively. In the above equations, the principle of virtual work was used to evaluate the rotation at the left end section of the beam, first term in Eq.(16b), and the displacement of the controlling point, Eq. (16d).

Horizontal displacement $u_{r1,k}$ at the left end section of the external reinforcement (see Eq. (16c)) is also unknown.

Interface slips $\boldsymbol{\Delta}_k = [\Delta_{1,k} \quad \dots \quad \Delta_{N,k}]^T$ occurring at each node of the interface can then be derived as follows, function of the sections displacements and rotations above determined:

$$\boldsymbol{\Delta}_k = -\mathbf{u}_{b,k} - \boldsymbol{\theta}_{b,k}(y_G + y_R) + \mathbf{u}_{r,k} \tag{17}$$

The final system of $N + 2$ nonlinear equations reads:

$$\mathbf{Z}(\mathbf{Y}) = \begin{bmatrix} \boldsymbol{\psi}(\mathbf{Y}) \\ \Psi_1(\mathbf{Y}) \\ \Psi_2(\mathbf{Y}) \end{bmatrix} = \begin{bmatrix} \boldsymbol{\Delta}_k(\mathbf{s}_k, \alpha_k, u_{r1,k}) - \mathbf{s}_k \\ N_{rN,k}(\mathbf{s}_k) \\ v_{bm,k}(\mathbf{s}_k, \alpha_k) - \delta_{m,k} \end{bmatrix} = \begin{bmatrix} \mathbf{0} \\ 0 \\ 0 \end{bmatrix}, \text{ where } \mathbf{Y} = \begin{bmatrix} \mathbf{s}_k \\ \alpha_k \\ u_{r1,k} \end{bmatrix} \tag{18}$$

The above equations, nonlinear due to the softening nature of the cohesive law and to the nonlinear behavior of both beam and reinforcement, impose kinematic compatibility at the interface (N equations), zero axial force at the external reinforcement end section (1

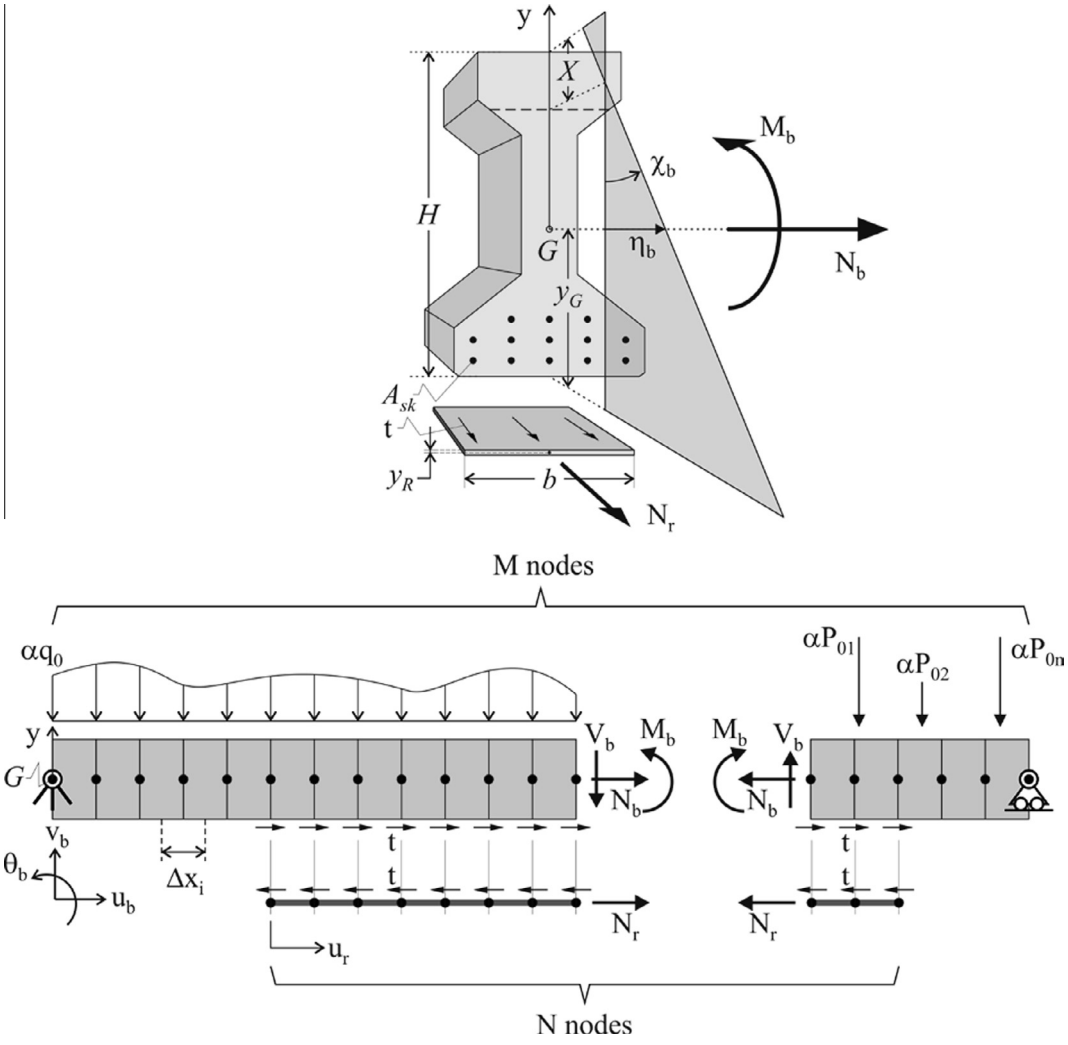

Fig. 7. Schematic representation of the discretized externally reinforced beam.

equation) and the assigned displacement at the controlling point (1 equation).

The solution at the *k-th* loading step has to be achieved by means of an iterative procedure. Initial trial values of the unknowns, i.e. α_k, $u_{r1,k}$ and vector $\mathbf{s}_k$, have to be assigned at the beginning of each loading step k (usually consisting with the solution of the previous step $k-1$) and then the following Newton–Raphson iteration procedure (run by index n) is adopted till convergence:

$$\mathbf{Y}_{n+1} = \mathbf{Y}_n - \left[\frac{\partial \mathbf{Z}}{\partial \mathbf{Y}}\bigg|_n\right]^{-1} \mathbf{Z}(\mathbf{Y}_n) \tag{19}$$

where $\mathbf{Y}$ is the vector of the unknowns and $\mathbf{Z}(\mathbf{Y})$ the vector of residuals. Consistent tangent operator $\frac{\partial \mathbf{Z}}{\partial \mathbf{Y}}$ is derived in Appendix A.

It is interesting to note that amplification load parameter α can be applied to any type of loading conditions; therefore, the numerical approach proposed can deal with displacement-controlled analyses with both concentrated and distributed forces.

It is important to underline that the problem cannot be formulated in terms of interface shear stresses **t**, in view of the softening behavior of the cohesive law. On the contrary, the choice of considering the interface slips **s** as primary unknowns allows to follow the reinforcement debonding and to model the entire equilibrium path from the response of the reinforced beam to that of the original one after detachment.

3. Validation of the numerical method

In order to validate the proposed formulation for modeling debonding in externally reinforced beams, benchmarking experimental tests taken from literature, concerning reinforced concrete beams, are simulated.

The experimental tests performed by Maalej et al., see [37], are here considered. They consist in five simple supported reinforced concrete beams, loaded in four point bending configuration. All the details about geometry, internal and external reinforcement can be found in Table 1 and Fig. 8.

In all experimental tests, debonding started from the reinforcement end due to the shear stress concentration occurring at the CFRP-concrete interface. The four reinforced beams (one is the reference one, i.e. without any external reinforcement) were characterized by a different CFRP reinforcement thickness, which induced different shear stress concentrations and consequently different failure loads. These failure mechanisms were correctly predicted by the current model, which, on the contrary, being

based on the beam hypothesis, would not be able to predict debonding phenomena starting from a stress concentration occurring in correspondence of a mid-flexural shear crack.

Figs. 9 and 10 visualize the surfaces representing curvature and axial strain as functions of bending moment and axial force for the concrete beam section, determined following the method described in Section 2.2.

Since in [37] no information are provided on the ultimate strain and on the shape of the steel reinforcement stress–strain relationship, it was decided to calibrate the adopted linear hardening constitutive law, through a tuning procedure with respect to the load–displacement curve of the reference beam (beam 1). The results achieved, reported in Table 2, permitted to reach a very good agreement with the experimental curve, see curves with index 1 in Fig. 11.

The rather small value of the identified Young modulus (the nominal value reported in [37] is 183.6 GPa) may be due to a compensation intrinsic in the solution of the inverse problem with respect to experimental data which may be affected by the testing machine deformability.

By means of a similar best fitting procedure with respect to beam 5 (the one having the thicker CFRP reinforcement) the cohesive properties, which cannot be measured directly, were identified, see Table 3. This identification allowed a good agreement with the experimental curve in terms of stiffness, ultimate load and post peak branch (see curves with index 5 in Fig. 11).

The material parameters above identified were then adopted to simulate the other reinforced beams (i.e. beam 2, 3 and 4), which were characterized by a different CFRP lamina thickness.

In Fig. 11, it is shown that the numerical method proposed is able to predict fairly well the experimental behavior of all the tested beams (not only those that had been used to identify the material properties), both in terms of stiffness and ultimate load (depicted in the curve by a circle or a square). For beams 3, 4 and 5, the failure mode consisted in ripping of the concrete cover due to external reinforcement debonding and the numerical method was also able to follow the descending branch. Beam 2 had the thinner CFRP reinforcement and both experimentally and numerically failed for CFRP rupture. The error obtained when simulating its load-carrying capacity is anyway small, and probably depends on the difference between the actual local strength of the CFRP sheet and the nominal one (i.e. the one adopted in the computations, equal to 3400 MPa according to [37]).

Table 1
Details of the external reinforcement of the five beams tested in [37].

Specimen	Beam 1	Beam 2	Beam 3	Beam 4	Beam 5
Number of layers	0	1	2	3	4
CFRP thickness (mm)	0	0.111	0.222	0.333	0.444

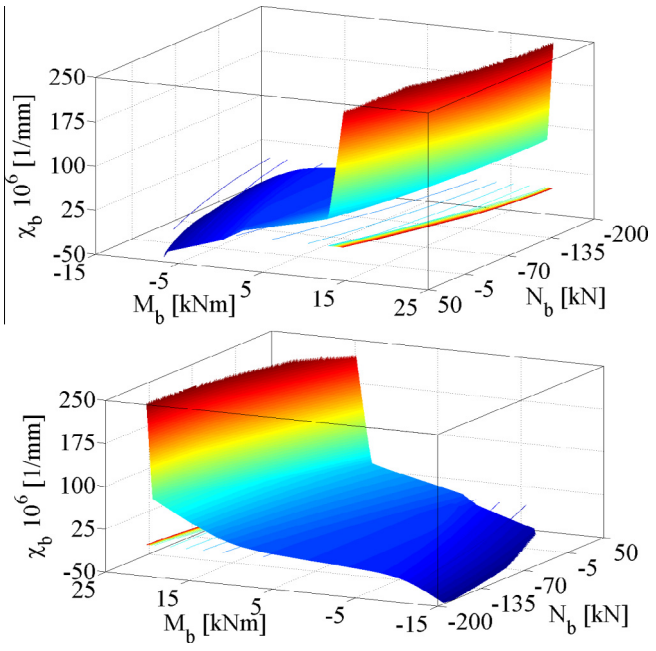

Fig. 9. Concrete beam curvature as function of bending moment and axial force.

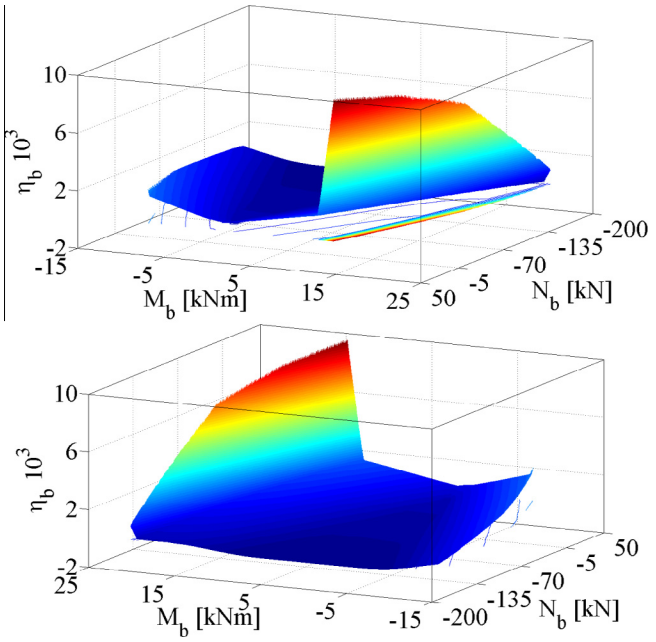

Fig. 10. Concrete beam axial deformation as function of bending moment and axial force.

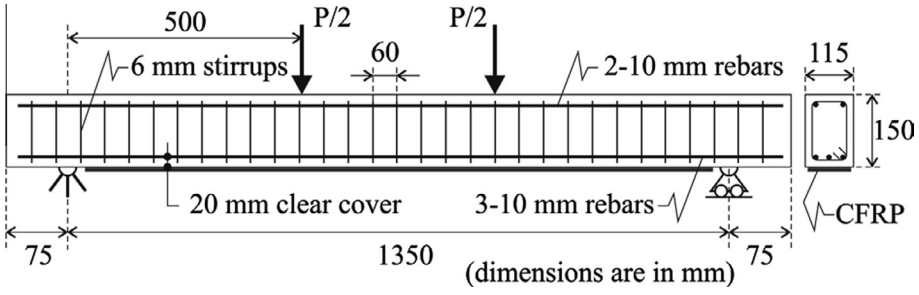

Fig. 8. Specimen geometry of the experimental tests by Maalej et al. [37].

Table 2
Identified steel reinforcement properties.

E_s	f_{sy}	H_s
165,240 MPa	561 MPa	1098 MPa

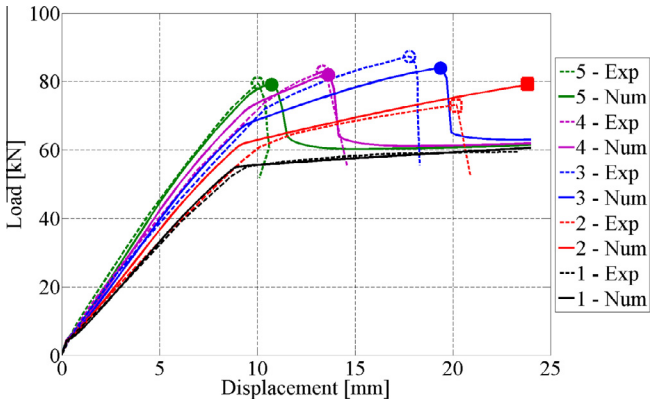

Fig. 11. Comparison between numerical and experimental load displacement curves. Failure mechanisms consist in both external reinforcement debonding (circle) and CFRP rupture (square).

Table 3
Identified interface properties entering the adopted bilinear cohesive law.

K_f	t_f	G_f
2.50 N/mm^3	0.97 MPa	1.08 N/mm

Fig. 12 visualizes the CFRP axial stress distribution, for all the four reinforced beams, along the longitudinal axis, computed in correspondence of the numerical ultimate load. In relation to beam 2, a maximum CFRP axial stress is reached, equal to the assumed nominal tensile strength reported in [37] (3400 MPa), coherently with the failure mechanism predicted by the numerical model and occurred in the test.

4. Parametric study

This Section is intended to present some parametric analyses aimed at showing the effect of the main design parameters on the overall behavior of a RC beam externally retrofitted in bending by a CFRP lamina. In order to emphasize the effects on the ultimate load of the parameters related to the external reinforcement and the adhesive, concrete was treated as linear elastic in compression, while the tensile behavior was assumed linear elastic up to the tensile strength f_{ct}, followed by brittle failure. Similarly, the strength of the CFRP lamina is set to be so high not to have its breaking before debonding.

The reference case considered is a simple supported beam 2.0 m long loaded by a uniform distributed load and reinforced by a CFRP lamina, 100 mm wide and 1.0 mm thick. The beam has a rectangular cross section with dimensions 100 mm x 200 mm, it is reinforced with rebars, whose total area is 402 mm^2 at the lower side, and 157 mm^2 at the upper side, see Fig. 13.

Parametric studies were performed with respect to the following parameters: CFRP lamina length L_r, fracture energy G_f, interface shear strength t_f and CFRP modulus of elasticity E_r, by varying each parameter at time with respect to the reference values reported in Table 4.

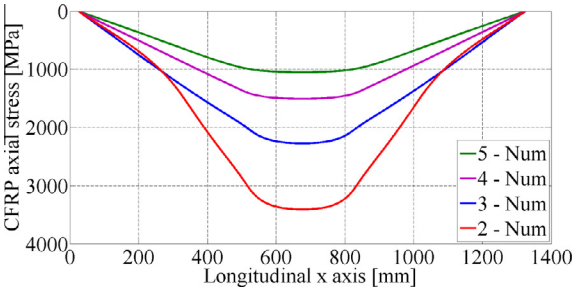

Fig. 12. CFRP axial stress in the four reinforced beams at their ultimate numerical load.

Fig. 14 visualizes the response of the reinforced beam with respect to a variation of the reinforcement length L_r within the range [1.0–1.8 m]. It turned out that the longer the reinforcement lamina, the higher the ultimate load and the more brittle the debonding phenomenon occurs, due to a larger amount of deformation energy stored in the beam.

Fig. 15 reports the parametric analysis performed with respect to the fracture energy G_f, made considering values comprised between 1.0 N/mm and 2.0 N/mm. It is shown that the higher the fracture energy the higher the ultimate load and the more ductile the debonding failure mechanism is. For fracture energy values smaller than the 1.0 N/mm, the curve presented a snap-back behavior and, therefore, the implemented method was not able to follow the response of the reinforced beam after debonding.

Fig. 16 visualizes the parametric analysis performed with respect to the interface shear strength t_f, considering values in the range [0.5–1.5 MPa]. It is shown that the higher the interface shear strength the higher the ultimate load and the more brittle the debonding failure mechanism is. For interface shear strength higher than the 1.25 MPa, the curve presented a snap-back behavior and, therefore, the implemented method was not able to follow the post-peak response of the reinforced beam.

It is important to observe that the maximum attained load strongly depends on the interface shear strength. This seems to be in contrast with what generally stated by guidelines, see [22], according to which, if the minimum bond length is guaranteed then the maximum transferrable force depends on the fracture energy only. However, this concept is true for pull–push tests where the reinforcement is loaded with a uni-form axial force, but it is wrong in the present case where a variable bending moment distribution induces into the CFRP lamina a non-uniform axial force. Indeed, if we considered a reinforced beam loaded in a four points bending configuration in such a way the CFRP lamina is in between the two loading points, then it would be possible to show that in this case the maximum load would not depend anymore on the interface shear strength.

The effect of the modulus of elasticity E_r on the response of the reinforced beam is similar to that of the lamina thickness h as emerged in Section 3. Fig. 17 shows that an increment of E_r causes the decreases of both the ultimate load and displacement. Indeed, the stiffer reinforcement induces a higher shear stress concentration at the reinforcement end and, consequently, a premature failure.

5. Closing remarks

In the present paper, a novel numerical approach, based on a modified version of the force method, was proposed to model the response of concrete beams externally strengthened in bending,

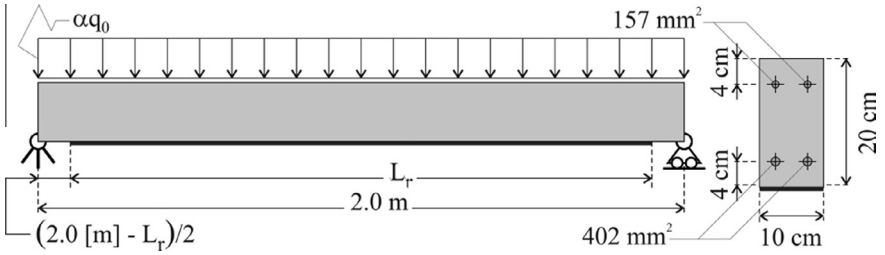

Fig. 13. Reference beam studied in the parametric analysis.

Table 4
Material properties and reinforcement length assumed as reference case in the parametric analysis.

Concrete	$E_c = 28,960$ MPa, $f_{ct} = 2.6$ MPa
Steel	$E_s = 210,000$ MPa, $f_{sy} = 450$ MPa, $H_s = 1035$ MPa
CFRP	$E_r = 230,000$ MPa, $L_r = 1.80$ m
Interface	$K_f = 2.5$ N/mm^3, $t_f = 1.0$ MPa, $G_f = 1.0$ N/mm

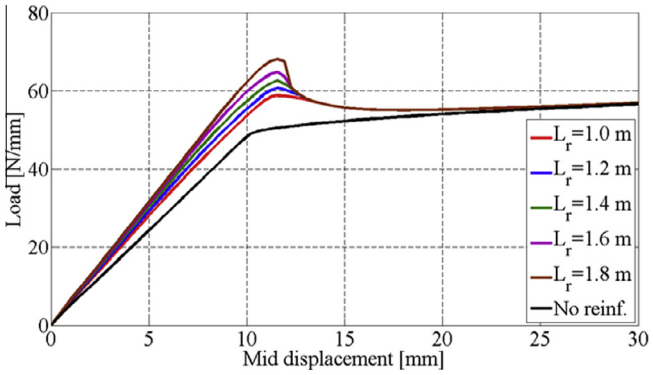

Fig. 14. Parametric study with respect to the reinforcement length L_r.

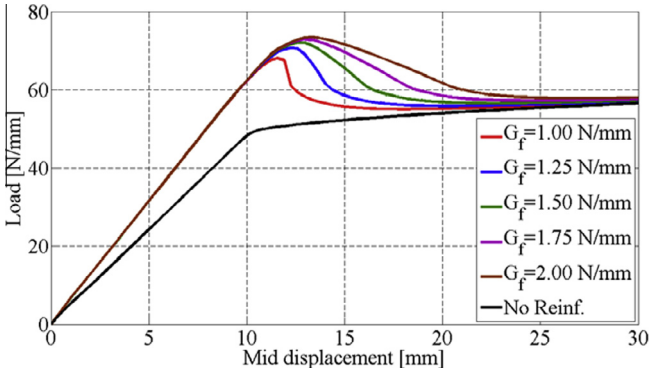

Fig. 15. Parametric study with respect to the fracture energy G_f.

up to the complete detachment of the CFRP lamina and further on. The method is able to follow the complete equilibrium path of the beam, from the response of the externally strengthened configuration to that of the original one after the debonding of the external reinforcement and the consequent and sudden load drop.

The numerical method is based on a cohesive approach to model the interface between the external reinforcement and the substrate, and on numerically built surfaces relating the

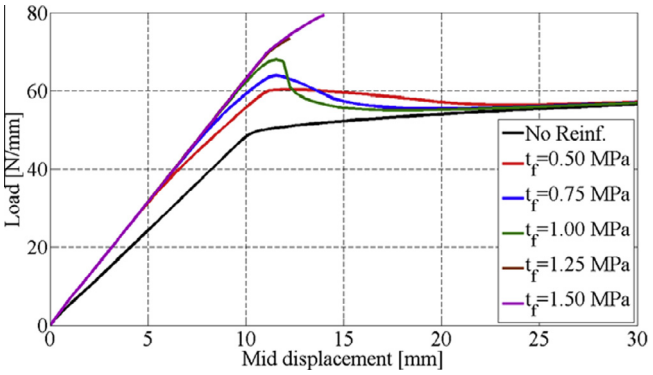

Fig. 16. Parametric study with respect to the interface shear strength t_f.

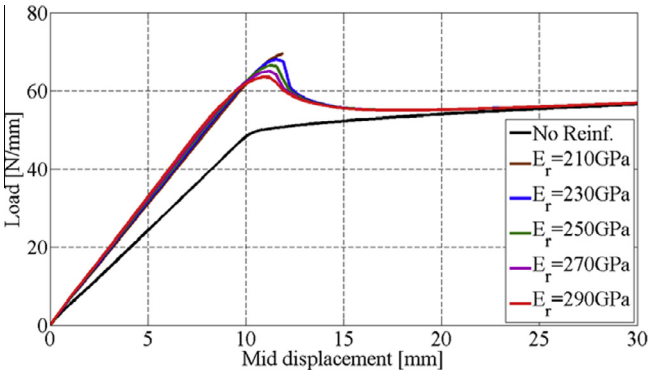

Fig. 17. Parametric study with respect to the modulus of elasticity E_r.

characteristics of deformation of the concrete beam (curvature and axial deformation) to the bending moment and axial force acting at each cross-section. The proposed approach is formulated considering concrete, steel rebar and external reinforcement as a nonlinear material. The formulation leads to a set of nonlinear equations expressed in terms of interface slips as primary unknowns.

The method turned out to be able to correctly estimate the results of experimental tests found in literature. The good agreement between experimental evidences and numerical simulations, means that the proposed approach may be considered as reference for design considerations.

To this purpose parametric analyses were performed on a classical reinforced concrete beam, strengthened with a CFRP lamina, in order to point out the effects on the response of the system of the main parameters involved in the strengthening design: reinforcement length, interface fracture energy, shear strength and CFRP elastic modulus.

Appendix A

Consistent tangent operator $\frac{\partial \mathbf{Z}}{\partial \mathbf{Y}}$ in Eq. (19) is derived in the following.

$$\left[\frac{\partial \mathbf{Z}}{\partial \mathbf{Y}}\right] = \begin{bmatrix} \frac{\partial \boldsymbol{\psi}}{\partial \mathbf{Y}} \\ \frac{\partial \Psi_1}{\partial \mathbf{Y}} \\ \frac{\partial \Psi_2}{\partial \mathbf{Y}} \end{bmatrix} \quad \text{where}: \quad \mathbf{Y} = \begin{bmatrix} \mathbf{s} \\ \alpha \\ u_{r1} \end{bmatrix} \tag{A1}$$

By applying the derivative chain rule, it follows that:

$$\begin{aligned} \frac{\partial \boldsymbol{\psi}}{\partial \mathbf{Y}} &= \frac{\partial \boldsymbol{\Delta}}{\partial \mathbf{Y}} - \frac{\partial \mathbf{s}}{\partial \mathbf{Y}} = \frac{\partial \boldsymbol{\Delta}}{\partial \mathbf{u}_b}\frac{\partial \mathbf{u}_b}{\partial \mathbf{Y}} + \frac{\partial \boldsymbol{\Delta}}{\partial \boldsymbol{\theta}_b}\frac{\partial \boldsymbol{\theta}_b}{\partial \mathbf{Y}} + \frac{\partial \boldsymbol{\Delta}}{\partial \mathbf{u}_r}\frac{\partial \mathbf{u}_r}{\partial \mathbf{Y}} - \frac{\partial \mathbf{s}}{\partial \mathbf{Y}} \\ &= -\frac{\partial \mathbf{u}_b}{\partial \boldsymbol{\eta}_b}\left(\frac{\partial \boldsymbol{\eta}_b}{\partial \mathbf{M}_b}\left(\frac{\partial \mathbf{M}_b}{\partial \mathbf{t}}\frac{\partial \mathbf{t}}{\partial \mathbf{s}}\frac{\partial \mathbf{s}}{\partial \mathbf{Y}} + \frac{\partial \mathbf{M}_b}{\partial \alpha}\frac{\partial \alpha}{\partial \mathbf{Y}}\right) + \frac{\partial \boldsymbol{\eta}_b}{\partial \mathbf{N}_b}\frac{\partial \mathbf{N}_b}{\partial \mathbf{t}}\frac{\partial \mathbf{t}}{\partial \mathbf{s}}\frac{\partial \mathbf{s}}{\partial \mathbf{Y}}\right) \\ &\quad - (y_G + y_R)\frac{\partial \theta_b}{\partial \boldsymbol{\chi}_b}\left(\frac{\partial \boldsymbol{\chi}_b}{\partial \mathbf{M}_b}\left(\frac{\partial \mathbf{M}_b}{\partial \mathbf{t}}\frac{\partial \mathbf{t}}{\partial \mathbf{s}}\frac{\partial \mathbf{s}}{\partial \mathbf{Y}} + \frac{\partial \mathbf{M}_b}{\partial \alpha}\frac{\partial \alpha}{\partial \mathbf{Y}}\right) + \frac{\partial \boldsymbol{\chi}_b}{\partial \mathbf{N}_b}\frac{\partial \mathbf{N}_b}{\partial \mathbf{t}}\frac{\partial \mathbf{t}}{\partial \mathbf{s}}\frac{\partial \mathbf{s}}{\partial \mathbf{Y}}\right) \\ &\quad + \frac{\partial \mathbf{u}_r}{\partial u_{r1}}\frac{\partial u_{r1}}{\partial \mathbf{Y}} + \frac{\partial \mathbf{u}_r}{\partial \boldsymbol{\eta}_r}\frac{\partial \boldsymbol{\eta}_r}{\partial \mathbf{N}_r}\frac{\partial \mathbf{N}_r}{\partial \mathbf{t}}\frac{\partial \mathbf{t}}{\partial \mathbf{s}}\frac{\partial \mathbf{s}}{\partial \mathbf{Y}} - \frac{\partial \mathbf{s}}{\partial \mathbf{Y}} \end{aligned} \tag{A2}$$

$$\frac{\partial \Psi_1}{\partial \mathbf{Y}} = \frac{\partial N_{rN}}{\partial \mathbf{t}}\frac{\partial \mathbf{t}}{\partial \mathbf{s}}\frac{\partial \mathbf{s}}{\partial \mathbf{Y}} \tag{A3}$$

$$\frac{\partial \Psi_2}{\partial \mathbf{Y}} = \frac{\partial v_{bm}}{\partial \boldsymbol{\chi}_b}\frac{\partial \boldsymbol{\chi}_b}{\partial \mathbf{Y}} = \frac{\partial v_{bm}}{\partial \boldsymbol{\chi}_b}\left(\frac{\partial \boldsymbol{\chi}_b}{\partial \mathbf{M}_b}\left(\frac{\partial \mathbf{M}_b}{\partial \mathbf{t}}\frac{\partial \mathbf{t}}{\partial \mathbf{s}}\frac{\partial \mathbf{s}}{\partial \mathbf{Y}} + \frac{\partial \mathbf{M}_b}{\partial \alpha}\frac{\partial \alpha}{\partial \mathbf{Y}}\right) + \frac{\partial \boldsymbol{\chi}_b}{\partial \mathbf{N}_b}\frac{\partial \mathbf{N}_b}{\partial \mathbf{t}}\frac{\partial \mathbf{t}}{\partial \mathbf{s}}\frac{\partial \mathbf{s}}{\partial \mathbf{Y}}\right) \tag{A4}$$

where

- $\frac{\partial \boldsymbol{\chi}_b}{\partial \mathbf{M}_b}$, $\frac{\partial \boldsymbol{\chi}_b}{\partial \mathbf{N}_b}$, $\frac{\partial \boldsymbol{\eta}_b}{\partial \mathbf{M}_b}$, $\frac{\partial \boldsymbol{\eta}_b}{\partial \mathbf{N}_b}$ and $\frac{\partial \boldsymbol{\eta}_r}{\partial \mathbf{N}_r}$ are diagonal matrices, computed according to Section 2.2;
- $\frac{\partial \mathbf{t}}{\partial \mathbf{s}}$ is a diagonal matrix whose terms are determined by deriving analytically the adopted interface cohesive law (Eq. (4));
- $\frac{\partial \mathbf{u}_b}{\partial \boldsymbol{\eta}_b}$, $\frac{\partial \boldsymbol{\theta}_b}{\partial \boldsymbol{\chi}_b}$, $\frac{\partial \mathbf{u}_r}{\partial \boldsymbol{\eta}_r}$ are computed by derivation of Eq. (16);
- $\frac{\partial \mathbf{M}_b}{\partial \mathbf{t}}$, $\frac{\partial \mathbf{N}_b}{\partial \mathbf{t}}$, $\frac{\partial \mathbf{N}_r}{\partial \mathbf{t}}$ are lower triangular matrices computed by deriving Eq. (14);
- $\frac{\partial \mathbf{s}}{\partial \mathbf{Y}}$, $\frac{\partial \alpha}{\partial \mathbf{Y}}$, $\frac{\partial u_{r1}}{\partial \mathbf{Y}}$ are Boolean matrices and vectors of 0 and 1, defined as follows ($\mathbf{I}$ and $\mathbf{0}$ being the identity and zero matrices, respectively):

$$\frac{\partial \mathbf{s}}{\partial \mathbf{Y}} = [\,\mathbf{I}_{N\times N} \quad \mathbf{0}_{N\times 2}\,]_{N\times(N+2)}, \quad \frac{\partial \alpha}{\partial \mathbf{Y}} = [\,0 \quad \cdots \quad 0 \quad 1 \quad 0\,]_{1\times(N+2)},$$
$$\frac{\partial u_{r1}}{\partial \mathbf{Y}} = [\,0 \quad \cdots \quad 0 \quad 1\,]_{1\times(N+2)}$$

References

[1] Bakis CE, Bank LC, Brown VL, Cosenza E, Davalos JF, Lesko JJ, et al. Fiber-reinforced polymer composites for construction state-of-the-art review. ASCE J Compos Constr 2002;6(2):73–87.
[2] Zhao XL, Zhang L. State-of-the-art review on FRP strengthened steel structures. Eng Struct 2007;29:1808–23.
[3] Teng JG, Yu T, Fernando D. Strengthening of steel structures with fiber-reinforced polymer composites. J Constr Steel Res 2012;78:131–43.
[4] Holloway LC, Cadei J. Progress in the technique of upgrading metallic structures with advanced polymer composites. Prog Struct Eng Mater 2002;4(2):131–48.
[5] Pisani MA. Evaluation of bending strength of RC beams strengthened with FRP sheets. ASCE J Compos Constr 2006;10(4):313–20.
[6] Bocciarelli M, di Feo C, Nisticò N, Pisani MA, Poggi C. Failure of RC beams strengthened in bending with unconventionally arranged CFRP laminates. Compos Part B 2013;54:246–54.
[7] Deng J, Lee MMK. Behaviour under static loading of metallic beams reinforced with a bonded CFRP plate. Compos Struct 2007;78:232–42.
[8] Chen JF, Teng JG. Shear capacity of FRP strengthened RC beams: FRP rupture. J Struct Eng 2003;129(5):615–25.
[9] Chen JF, Teng JG. Shear capacity of FRP strengthened RC beams: FRP debonding. Constr Build Mater 2003;1(17):27–41.
[10] Bocciarelli M, Gambarelli S, Nisticò N, Pisani MA, Poggi C. Shear behavior of RC elements strengthened with steel profiles and CFRP wraps. Compos Part B 2014;67:9–21.
[11] Zhao XL, Al-Mahaidi R. Web buckling of light steel beams strengthened with CFRP subjected to end-bearing forces. Thin Walled Struct 2009;47(10): 1029–36.
[12] Colombi P, Poggi C. Strengthening of tensile steel members and bolted joints using adhesively bonded CFRP plates. Constr Build Mater 2006;20:22–33.
[13] Matta F, Karbhari VM, Vitaliani R. Tensile response of steel/CFRP adhesive bonds for the rehabilitation of civil structures. Struct Eng Mech 2005;20(5): 589–608.
[14] Bocciarelli M, Colombi P, Fava G, Poggi C. Interaction of interface delamination and plasticity in tensile steel members reinforced by CFRP plates. Int J Fract 2007;146:79–92.
[15] Colombi P, Fava G. Fatigue behaviour of tensile steel/CFRP joints. Compos Struct 2012;94:2407–17.
[16] Monti G, Nisticò N. Square and rectangular concrete columns confined by CFRP: experimental and numerical investigation. Mech Compos Mater 2008;44(3):289–308.
[17] Realfonzo R, Napoli A. Concrete confined by FRP systems: confinement efficiency and design strength models. Compos Part B 2011;42(4):736–55.
[18] Abdel Baky H, Ebead UA, Neale KW. Nonlinear micromechanics-based bond-slip model for FRP/concrete interfaces. Eng Struct 2012;39:11–23.
[19] Akbar I, Oehlers DJ, Mohamed Ali MS. Derivation of the bond-slip characteristics for FRP plated steel members. J Constr Steel Res 2010;66: 1047–56.
[20] Mazzotti C, Savoia M, Ferracuti B. An experimental study on delamination of FRP plates bonded to concrete. Constr Build Mater 2008;22:1409–21.
[21] Colombi P, Fava G, Poggi C. End debonding of CFRP wraps and strips for the strengthening of concrete structures. Compos Struct 2014;111:510–21.
[22] National Research Council, CNR-DT200 R1/2012. Guide for the design and construction of externally bonded FRP systems for strengthening existing structures. Italy; 2012.
[23] ACI 440.2R-02. Guide for design and construction of externally bonded FRP systems for strengthening concrete structures. American Concrete Institute, Committee; 2002.
[24] Martinelli E, Napoli A, Nunziata B, Realfonzo R. A 1D finite element model for the flexural behaviour of RC beams strengthened with MF-FRP strips. Compos Struct 2014;107:190–204.
[25] Yu Y, Chiew SP, Lee CK. Bond failure of steel beams strengthened with FRP laminates – Part 2: Verification. Compos Part B 2011;42:1122–34.
[26] Chen GM, Teng JG, Chen JF. Finite-element modeling of intermediate crack debonding in FRP-plated RC beams. ASCE J Compos Constr 2011;15:339–53.
[27] Seleem MH, Sharaky IA, Sallam HEM. Flexural behavior of steel beams strengthened by carbon fiber reinforced polymer plates – three dimensional finite element simulation. Mater Des 2010;31:1317–24.
[28] Linghoff D, Al-Emrani M. Performance of steel beams strengthened with CFRP laminate – Part 2: FE analyses. Compos Part B 2010;41:516–22.
[29] Hawileh RA, Naser MZ, Abdalla JA. Finite element simulation of reinforced concrete beams externally strengthened with short-length CFRP plates. Compos Part B 2013;45(1):1722–30.
[30] Ranzi G. Locking problems in the partial interaction analysis of multi-layered composite beams. Eng Struct 2008;30(10):2900–11.
[31] Ranzi G, Leoni G, Zandonini R. State of the art on the time-dependent behaviour of composite steel-concrete structures. J Constr Steel Res 2013;80:252–63.
[32] UNI EN 1992-1-1:2005, Eurocode 2 – Design of concrete structures. Part 1-1: General rules and rules for buildings. Brussels, Belgium; 2005.
[33] Rotter JM. Rapid exact inelastic biaxial bending analysis. J ASCE Struct Div 1985;111:2659–74.
[34] Pisani MA. A numerical method to analyse compact cross sections. Comput Struct 1996;59(6):1063–72.
[35] Malerba PG. Numerical aspects of the analysis of reinforced concrete sections bending and compression (in Italian). Atti del Congresso C. T. E. sulla Industrializzazione Edilizia; 1984. p. 165–71.
[36] CEB/FIP, Manual of Buckling and Instability, Bulletin d'Information N.123, The International Federation for Structural Concrete editor; 1977.
[37] Maalej M, Bian Y. Interfacial shear stress concentration in FRP-strengthened beams. Compos Struct 2001;54:417–26.